In vivo feasibility of endovascular Doppler optical coherence tomography

Cuiru Sun,[1,6] Felix Nolte,[1,2,6] Kyle H. Y. Cheng,[1,3] Barry Vuong,[1] Kenneth K. C. Lee,[1,3] Beau A. Standish,[1,2] Brian Courtney,[4] Thomas R. Marotta,[5] Adrian Mariampillai,[1] and Victor X. D. Yang[1,3,5,*]

[1]Biophotonics and Bioengineering Laboratory, Dept. Electrical and Computer Engineering, Ryerson University, 350 Victoria St. Toronto, ON, M5B2K3 Canada
[2]Faculty of Electrical Engineering and Information Technology, University of Applied Sciences, Karlsruhe, Moltkestraße 30, 76133 Karlsruhe, Germany
[3]Dept. Electrical and Computer Engineering, University of Toronto, 27 King's College Circle, Toronto, Ontario, M5S 1A1, Canada
[4]Colibri Technologies Inc., 3080 Yonge Street, Toronto, ON, M4N 3N1, Canada
[5]Dept. of Medical Imaging, St. Michael's Hospital, 30 Bond Street, Toronto, ON, M5B 1W8, Canada
[6]These authors contributed equally to this work.
*yangv@ee.ryerson.ca

Abstract: Feasibility of detecting intravascular flow using a catheter based endovascular optical coherence tomography (OCT) system is demonstrated in a porcine carotid model *in vivo*. The effects of A-line density, radial distance, signal-to-noise ratio, non-uniform rotational distortion (NURD), phase stability of the swept wavelength laser and interferometer system on Doppler shift detection limit were investigated in stationary and flow phantoms. Techniques for NURD induced phase shift artifact removal were developed by tracking the catheter sheath. Detection of high flow velocity (~51 cm/s) present in the porcine carotid artery was obtained by phase unwrapping techniques and compared to numerical simulation, taking into consideration flow profile distortion by the eccentrically positioned imaging catheter. Using diluted blood in saline mixture as clearing agent, simultaneous Doppler OCT imaging of intravascular flow and structural OCT imaging of the carotid artery wall was feasible. To our knowledge, this is the first *in vivo* demonstration of Doppler imaging and absolute measurement of intravascular flow using a rotating fiber catheter in carotid artery.

© 2012 Optical Society of America

OCIS codes: (170.4500) Optical coherence tomography; (170.3880) Medical and biological imaging; (280.3340) Laser Doppler velocimetry; (120.5050) Phase measurement.

References and links

1. N. Suwanwela, U. Can, K. L. Furie, J. F. Southern, N. R. Macdonald, C. S. Ogilvy, C. J. Hansen, F. S. Buonanno, W. M. Abbott, W. J. Koroshetz, and J. P. Kistler, "Carotid Doppler ultrasound criteria for internal carotid artery stenosis based on residual lumen diameter calculated from *en bloc* carotid endarterectomy specimens," Stroke **27**(11), 1965–1969 (1996).
2. A. V. Kamenskiy, Y. A. Dzenis, J. N. Mactaggart, A. S. Desyatova, and I. I. Pipinos, "*In vivo* three-dimensional blood velocity profile shapes in the human common, internal, and external carotid arteries," J. Vasc. Surg. **54**(4), 1011–1020 (2011).
3. J. W. Doucette, P. D. Corl, H. M. Payne, A. E. Flynn, M. Goto, M. Nassi, and J. Segal, "Validation of a Doppler guide wire for intravascular measurement of coronary artery flow velocity," Circulation **85**(5), 1899–1911 (1992).
4. D. H. Koschyk, C. W. Hamm, and T. Meinertz, "Colour coded blood flow imaging in intravascular ultrasound," Heart **84**(4), 376 (2000).
5. W. G. Li, A. F. W. van der Steen, C. T. Lancée, I. Céspedes, and N. Bom, "Blood flow imaging and volume flow quantitation with intravascular ultrasound," Ultrasound Med. Biol. **24**(2), 203–214 (1998).
6. C. Petersen, D. Adler, and J. Schmitt, "Clinical studies of frequency domain optical coherence tomography in the coronary arteries: the first 2000 patients," Proc. SPIE **7548**, 75483H (2010).

7. X. Li, T. H. Ko, and J. G. Fujimoto, "Intraluminal fiber-optic Doppler imaging catheter for structural and functional optical coherence tomography," Opt. Lett. **26**(23), 1906–1908 (2001).
8. J. A. Izatt, M. D. Kulkarni, S. Yazdanfar, J. K. Barton, and A. J. Welch, "*In vivo* bidirectional color Doppler flow imaging of picoliter blood volumes using optical coherence tomography," Opt. Lett. **22**(18), 1439–1441 (1997).
9. H. Ren, Z. Ding, Y. Zhao, J. Miao, J. S. Nelson, and Z. Chen, "Phase-resolved functional optical coherence tomography: simultaneous imaging of *in situ* tissue structure, blood flow velocity, standard deviation, birefringence, and Stokes vectors in human skin," Opt. Lett. **27**(19), 1702–1704 (2002).
10. B. J. Vakoc, S. H. Yun, J. F. de Boer, G. J. Tearney, and B. E. Bouma, "Phase-resolved optical frequency domain imaging," Opt. Express **13**(14), 5483–5493 (2005).
11. A. M. Rollins, S. Yazdanfar, R. Ung-Arunyawee, and J. A. Izatt, "Real time color Doppler optical coherence tomography using a novel autocorrelation technique," in *Summaries of Papers Presented at the Conference on Lasers and Electro-Optics, 1999. CLEO '99* (IEEE, 1999), 451–452.
12. V. X. D. Yang, M. L. Gordon, A. Mok, Y. Zhao, Z. Chen, R. S. C. Cobbold, B. C. Wilson, and I. Alex Vitkin, "Improved phase-resolved optical Doppler tomography using the Kasai velocity estimator and histogram segmentation," Opt. Commun. **208**(4-6), 209–214 (2002).
13. K. H. Y. Cheng, C. R. Sun, J. P. Cruz, T. R. Marotta, J. Spears, W. J. Montanera, P. R. Herman, A. Thind, B. Courtney, B. A. Standish, and V. X. D. Yang, "Feasibility of endovascular optical coherence tomography for high-resolution carotid vessel wall imaging," Proc. SPIE **8207**, 82074N, 82074N-12 (2012).
14. K. H. Cheng, C. Sun, J. P. Cruz, T. R. Marotta, J. Spears, W. J. Montanera, A. Thind, B. Courtney, B. A. Standish, and V. X. Yang, "Comprehensive data visualization for high resolution endovascular carotid arterial wall imaging," J. Biomed. Opt. **17**(5), 056003 (2012).
15. V. X. D. Yang, M. L. Gordon, B. Qi, J. Pekar, S. Lo, E. Seng-Yue, A. Mok, B. C. Wilson, and I. A. Vitkin, "High speed, wide velocity dynamic range Doppler optical coherence tomography (Part I): System design, signal processing, and performance," Opt. Express **11**(7), 794–809 (2003).
16. K. K. C. Lee, A. Mariampillai, J. X. Z. Yu, D. W. Cadotte, B. C. Wilson, B. A. Standish, and V. X. D. Yang, "Real-time speckle variance swept-source optical coherence tomography using a graphics processing unit," Biomed. Opt. Express **3**(7), 1557–1564 (2012).
17. D. J. Smithies, T. Lindmo, Z. P. Chen, J. S. Nelson, and T. E. Milner, "Signal attenuation and localization in optical coherence tomography studied by Monte Carlo simulation," Phys. Med. Biol. **43**(10), 3025–3044 (1998).
18. G. van Soest, J. G. Bosch, and A. F. W. van der Steen, "Azimuthal registration of image sequences affected by nonuniform rotation distortion," IEEE Trans. Inf. Technol. Biomed. **12**(3), 348–355 (2008).
19. G. J. Tearney, E. Regar, T. Akasaka, T. Adriaenssens, P. Barlis, H. G. Bezerra, B. Bouma, N. Bruining, J. M. Cho, S. Chowdhary, M. A. Costa, R. de Silva, J. Dijkstra, C. Di Mario, D. Dudek, E. Falk, M. D. Feldman, P. Fitzgerald, H. M. Garcia-Garcia, N. Gonzalo, J. F. Granada, G. Guagliumi, N. R. Holm, Y. Honda, F. Ikeno, M. Kawasaki, J. Kochman, L. Koltowski, T. Kubo, T. Kume, H. Kyono, C. C. S. Lam, G. Lamouche, D. P. Lee, M. B. Leon, A. Maehara, O. Manfrini, G. S. Mintz, K. Mizuno, M. A. Morel, S. Nadkarni, H. Okura, H. Otake, A. Pietrasik, F. Prati, L. Räber, M. D. Radu, J. Rieber, M. Riga, A. Rollins, M. Rosenberg, V. Sirbu, P. W. J. C. Serruys, K. Shimada, T. Shinke, J. Shite, E. Siegel, S. Sonoda, M. Suter, S. Takarada, A. Tanaka, M. Terashima, T. Thim, S. Uemura, G. J. Ughi, H. M. M. van Beusekom, A. F. W. van der Steen, G. A. van Es, G. van Soest, R. Virmani, S. Waxman, N. J. Weissman, and G. Weisz; International Working Group for Intravascular Optical Coherence Tomography (IWG-IVOCT), "Consensus standards for acquisition, measurement, and reporting of intravascular optical coherence tomography studies: a report from the International Working Group for Intravascular Optical Coherence Tomography Standardization and Validation," J. Am. Coll. Cardiol. **59**(12), 1058–1072 (2012).
20. K. H. Y. Cheng, C. Sun, B. Vuong, K. K. C. Lee, A. Mariampillai, T. R. Marotta, J. Spears, W. J. Montanera, P. R. Herman, T.-R. Kiehl, B. A. Standish, and V. X. D. Yang, "Endovascular optical coherence tomography intensity kurtosis: visualization of vasa vasorum in porcine carotid artery," Biomed. Opt. Express **3**(3), 388–399 (2012).
21. C. Dennis, Ghiglia and M. D. Pritt, *Two-Dimensional Phase Unwrapping: Theory, Algorithms and Software* (Wiley-Interscience, New York, 1998).
22. R. S. C. Cobbold, *Foundations of Biomedical Ultrasound* (Oxford University Press, Oxford, 2007), p. 832.
23. S. G. Proskurin, I. A. Sokolova, and R. K. Wang, "Imaging of non-parabolic velocity profiles in converging flow with optical coherence tomography," Phys. Med. Biol. **48**(17), 2907–2918 (2003).
24. B. Rao, L. F. Yu, H. K. Chiang, L. C. Zacharias, R. M. Kurtz, B. D. Kuppermann, and Z. P. Chen, "Imaging pulsatile retinal blood flow in human eye," J. Biomed. Opt. **13**(4), 040505 (2008).
25. D. Morofke, M. C. Kolios, I. A. Vitkin, and V. X. Yang, "Wide dynamic range detection of bidirectional flow in Doppler optical coherence tomography using a two-dimensional Kasai estimator," Opt. Lett. **32**(3), 253–255 (2007).
26. J. Kalkman, A. V. Bykov, G. J. Streekstra, and T. G. van Leeuwen, "Multiple scattering effects in Doppler optical coherence tomography of flowing blood," Phys. Med. Biol. **57**(7), 1907–1917 (2012).
27. F. J. H. Gijsen, J. J. Wentzel, A. Thury, F. Mastik, J. A. Schaar, J. C. H. Schuurbiers, C. J. Slager, W. J. van der Giessen, P. J. de Feyter, A. F. W. van der Steen, and P. W. Serruys, "Strain distribution over plaques in human coronary arteries relates to shear stress," Am. J. Physiol. Heart Circ. Physiol. **295**(4), H1608–H1614 (2008).

1. Introduction

Blood flow velocity and volumetric flow measurements are important parameters for assessment of the severity of stenosis and the outcome of interventional therapy. Over the last two decades Duplex ultrasonogrophy [1,2] has become a routine imaging and measurement technique for the detection and clinical monitoring of carotid stenosis. Despite the inherent alteration of hemodynamics, as a consequence of physically placing a catheter in the coronary artery, intravascular ultrasound Doppler measurements [3] have been used for coronary blood flow measurements. Other ultrasound techniques such as color coded intravascular ultrasound blood flow imaging [4] and de-correlation based flow measurements [5] have been proposed to extract flow information from cross-sectional IVUS data and display simultaneous morphological data and flow information. Endovascular optical coherence tomography (OCT) has become an important modality for coronary stenosis imaging and stenting evaluation [6]. However, limited *in vivo* blood flow measurement has been conducted by endovascular OCT since the attempt by Li *et al.* [7] to measure the intraluminal velocity profile in a vessel phantom using a prototype OCT Doppler catheter. Using color Doppler [8], phase-resolved Doppler OCT [9,10], autocorrelation [11] or Kasai velocity estimation techniques [12] in a circumferentially scanning catheter probe carries its own unique challenges. These include dilution of blood by saline to improve OCT penetration, motion artifacts induced by the rotating optical probe, and the radially dependent noise background of measured Doppler signals. The widespread clinical use of the C7-XR OCT system (Lightlab Imaging, St. Jude Medical Inc. St. Paul, Minnesota, USA) would benefit from a technique compatible with rotational OCT catheters for Doppler imaging. In this paper we show preliminary results of *in vivo* intraluminal blood flow measurement using endovascular OCT in a porcine carotid model.

2. Materials and methods

Porcine carotid imaging protocols were approved by the Animal Care Committees of Sunnybrook Health Sciences Centre and St. Michael's Hospital, Toronto, Ontario, Canada, and described previously [13,14]. We noted the C7-XR OCT system has been applied to various endovascular structural imaging successfully with its high frame rate of 100 frames/s. However this results in a ~500 A-scans in each frame and contains insufficient overlap for adjacent pixels and thus the real-time velocity estimation by phase resolved methods could not be obtained accurately [15]. A custom-made data acquisition system [16] was combined with the C7-XR OCT system to acquire high-density A-line images at 20 frames/s rates that are suitable for Doppler shift calculation.

2.1 System configuration

The system used in this study consists of the C7-XR OCT system and a personal computer equipped with a data acquisition card (ATS9350, Alazartech) via PCIe x8 interface, a display card with graphics processing unit (GPU) for high speed computation (GeForce GTX 460 1GB, NVIDIA) over PCIe x16 interface and a solid state drive (Intel 510 Series 250GB) through SATA II interface. Figure 1(a) displays the interconnections between the hardware and the motherboard, and the connection between the personal computer and the back end of the C7-XR OCT system, which enabled raw OCT signal acquisition, saving and post-processing. The DAQ channels included a linear *k*-clock, the A-scan trigger, and the raw OCT signal. Previously developed custom software [16] was employed in this study with addition of minor modifications to accommodate the endovascular OCT system that provided a linear *k*-space sampling clock.

   The angle between the scanning beam and the axis of catheter (C7 Dragonfly, St. Jude Medical Inc. St. Paul, Minnesota, USA) was measured to be ~70° in air without water or saline injection from a measurement shown in Fig. 1(b). However, this angle may change
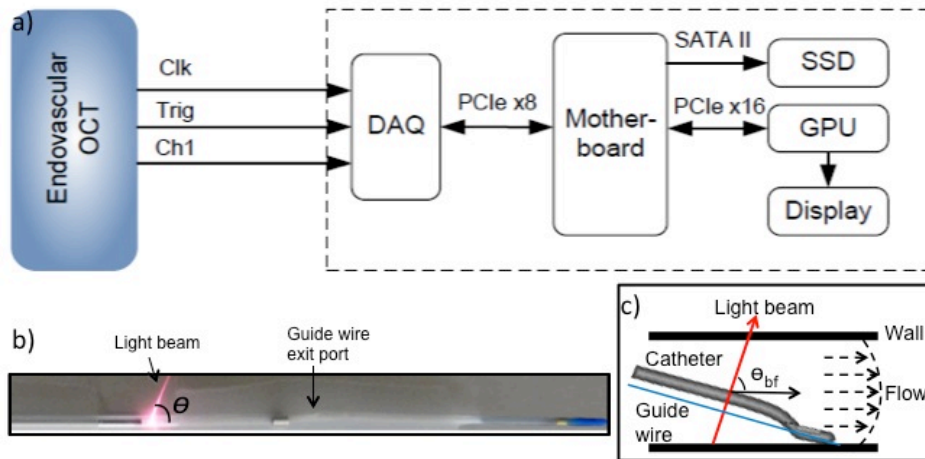
Fig. 1. Doppler imaging setup for endovascular OCT system. (a) High-speed data acquisition and graphics processor processing unit (GPU) processor connection to back end of C7-XR OCT system for high density A-line imaging. Clk: *k*-clock, Trig: A-scan trigger, Ch1: channel for raw OCT signal; DAQ: data acquisition; SSD: solid-state drive. (b) The imaging catheter showing the Doppler angle of the imaging beam, which is variable depending on the position of the guide wire and catheter location. (c) A schematic diagram showing the imaging catheter is not coaxial with the blood vessel. θ_{bf} indicates the beam-to-flow angle.

slightly during imaging due to refractive index variation of various mixing ratios of water,blood, contrast and saline. Moreover, in most cases, the imaging catheter is not coaxial with the blood vessel, as determined by the positions of the guide wire and image catheter. This non-coaxial orientation (shown in Fig. 1(c)) while in most cases creates non-perpendicularity between the beam and flow direction such that the Doppler signal induced by blood flow can be obtained also represents a source of error in determining the absolute flow velocity.

The flow velocity is calculated from Doppler shift obtained by Kasai autocorrelation [15]. The resulting measurement accuracy of blood flow depends on the size of the window used for Kasai calculation and the percentage of voxel overlap between adjacent A-lines. To optimize the radial and circumferential resolution, the percentage of overlap of the window is carefully chosen based on the axial point spread function (PSF) and spot size of the OCT system. The axial PSF at 3 dB is ~14 um in air, resulting in ~10 um in tissue, which degrades due to multiple scattering of photons and dispersion. However, previous research has shown that the variation of PSF remains minimal within blood vessels, for example, approximately 4% at an optical depth of 35 mean free path (mfp) [17]. The spot size and working distance (from the edge of the catheter) of the catheter are 25 um and ~1.5 mm respectively. The scanning beam diverges as the distance from the catheter is increased as shown in Fig. 2(a). The percentage of overlap of adjacent voxels according to the beam spots is plotted in Fig. 2(b). The four curves representing percentage of voxel overlap versus the distance from the catheter for 2500 A-lines/frame, 1250 A-lines/frame, 830 A-lines/frame and 500 A-lines/frame respectively. It can be seen that the pixels still have ~80% overlap at 4 mm away from the catheter at 2500 A-lines/frame, while the overlap percentage decreases with the decreasing the A-line density. Therefore 2500 A-line/frame images would be more suitable for accurate Doppler shift calculations. A 2×10 window (at depth and transverse directions relative to the optical beam) was chosen for Kasai autocorrelation calculation of Doppler shift to improve velocity detection sensitivity during Doppler processing.
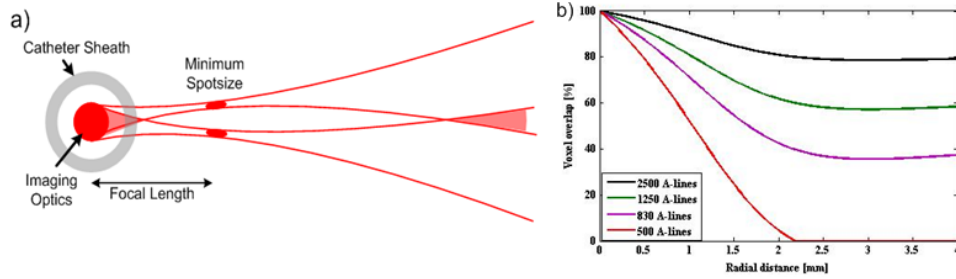
Fig. 2. (a) A schematic diagram showing the scanning beam from the imaging catheter. (b) Percentage of voxel overlap changes with the distance from the catheter for 2500 A-lines, 1250 A-lines, 830 A-lines and 500 A-lines per frame. The decline of voxel overlap between A-lines limits adequate imaging of Doppler shift.

2.2 Motion artifact of imaging catheter removal

Movement of the catheter induces artifact, which can be observed from the Doppler image of the sheath of the catheter. The rotation and axial motion of the fiber optic core within the catheter during endovascular imaging procedure also contribute to the detected Doppler image artifacts, and limit the minimal detectable velocity. Bending and twisting of the imaging catheter sheath, unavoidable during *in vivo* navigation of the catheter through the vasculature, can adversely couple with the high-speed rotation of the optic fiber and induce vibration. The vibration can introduce undesired relative motion (both radial and longitudinal) between the optic fiber and the catheter sheath. The resultant non-uniform rotational distortion (NURD) [18], when severe, can induce obvious artifacts in the structural imaging [19]. Phase sensitive imaging is more susceptible to such relative motion and significant phase shift artifact can exist without obvious structural imaging NURD.

To understand the NURD induced phase shift artifacts caused by the complex fiber motion and its effect on flow detection, a slow flow phantom was imaged with the Dragonfly catheter. Homogenously diluted mixture of blood (1.5% by volume) in saline, simulating imcompletely clearing of blood during saline flush, was injected to the flow phantom at 50 ml/hr (corresponding to 3.5 mm/s maximal flow velocity) using an infusion pump. The imaging results are shown in Fig. 3. Figure 3(a) is a structural image, from which the sheath and internal reflection of the imaging catheter can be observed. The catheter sheath, containing inner and outer surface reflections, can serve as reference surfaces for phase shift calibration against the phase artifacts. In addition, internal multiple reflection, such as those from the interface of focal elements in the fiber probe, may serve as phase shift calibration against phase instability in the swept source laser, interferometer and DAQ of the OCT system [10]. The Doppler shift generated in the internal reflection (red curve in Fig. 3(b)) is < 0.02 rad, therefore the phase instability induced error is negligible. The phase shift generated on the catheter sheath (black curve in Fig. 3(b)) is due to the NURD induced phase artifact as the catheter sheath is stable. Without removing the NURD artifacts, the slow flow rate induced Doppler shift is completely masked as shown in Fig. 3(c). The total Doppler shift detected in the flow region is a vector sum of the shift generated by the flowing particles and the shift produced by the moving fiber optic. From Fig. 3(c), it can be seen that the bulk-phase change induced by the oscillation of the fiber optic is constant along the radial direction. Therefore the fiber motion artifact can be eliminated by subtracting the Doppler shift measured on the sheath of the catheter. The corrected phase map is shown in Fig. 3(d), where the average Doppler shift of the flow is ~0.4 rad corresponding to flow velocity of 4 mm/s, which is comparable with the theoretical value.
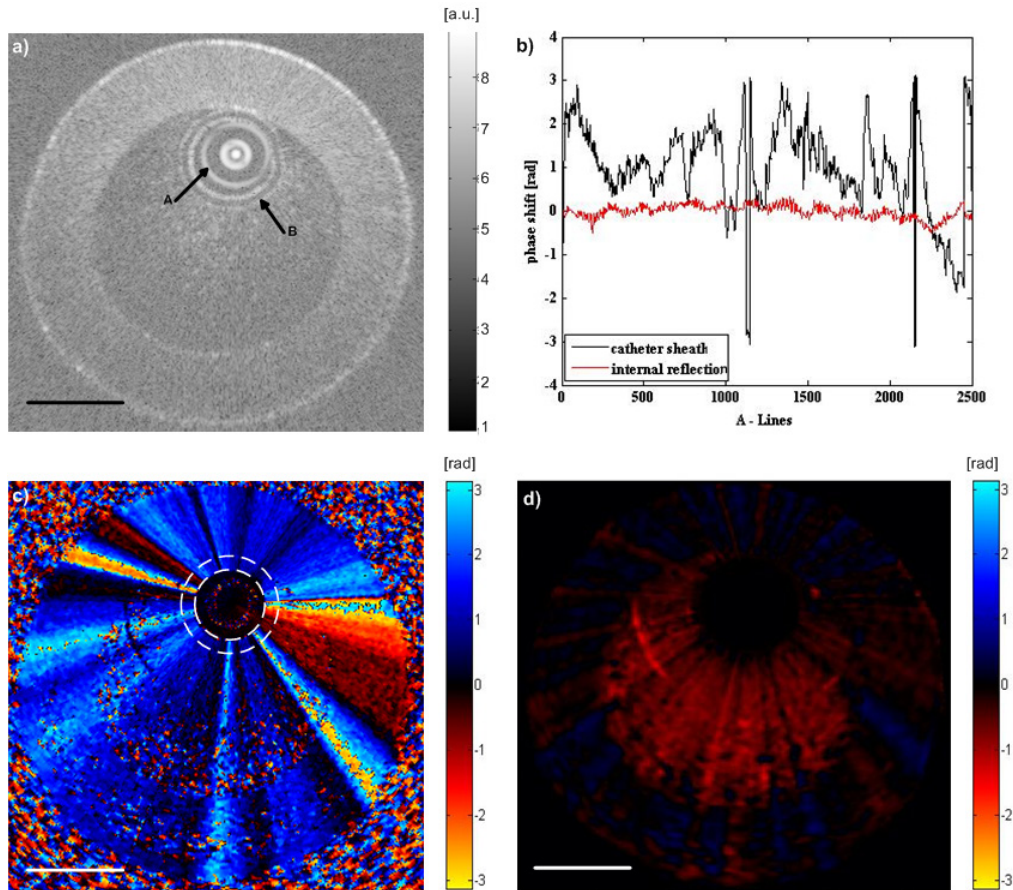
Fig. 3. Imaging of a slow flow phantom. (a) Structural image of 1.5% blood in saline mixture within the tube, where arrow A indicates the internal reflection of the imaging optics, and arrow B indicates the outer surface of the imaging catheter sheath. (b) Phase shift obtained from the internal reflection indicated by arrow A and catheter sheath indicated by arrow B in (a). The phase shift of the catheter sheath is the median of data along the catheter thickness. (c) Doppler shift image of the slow flow phantom. The dashed ring indicates the sheath of the imaging catheter, with phase shift induced by NURD in a radially constant manner throughout the image. (d) Doppler image after suppression of the motion artifact, which displays the phase shift induced by the slow flow inside the tube phantom. Scale bars = 1 mm.

2.3 Noise floor in Doppler shift measurement

During endovascular imaging, except for various motion artifacts, the density of A-lines and the angular line spaces increasing along the radius would also affect the Doppler shift calculation. A phantom was constructed to evaluate these effects. The phantom was made of gelatin with TiO_2 particles to model scatterers (concentration: 0.5 g/l). The concentration of TiO_2 was chosen to simulate relatively low SNR conditions that would be encountered during *in vivo* endovascular imaging, with incomplete clearing of blood in the vessel lumen. A tube with ~3 mm outer diameter was embedded to allow insertion of the OCT catheter. The Dragonfly OCT imaging catheter was advanced in the tube through a guide wire to the region of interest. Since there is no movement of the phantom, any nonzero phase shift detected during this procedure was attributed to measurement error. A cross-section of the phantom was imaged by both 2500 A-lines per frame and 500 A-lines per frame. Figures 4(a) and 4(b) demonstrate the structural and color Doppler images after removing bulk motion induced by catheter oscillation. Both images were acquired with 2500 A-lines per frame. The white sector

in Fig. 4(a) indicates a region of interest (ROI), where the Doppler shift was calculated as shown in Fig. 4(b). The standard deviation of the phase shift determines the minimal detectable phase change. This parameter varies with the radial distance and signal to noise ratio (SNR) of the OCT signal. Figures 4(c) and 4(d) show these relations for 2500 A-line per frame mode, and in comparison, 500 A-line per frame mode. The latter showed consistently higher noise floor in the phase measurement, and would not be suitable for *in vivo* measurements. When the radial distance from the catheter increases or when the SNR decreases, the phase measurement noise floor increases as expected [10].
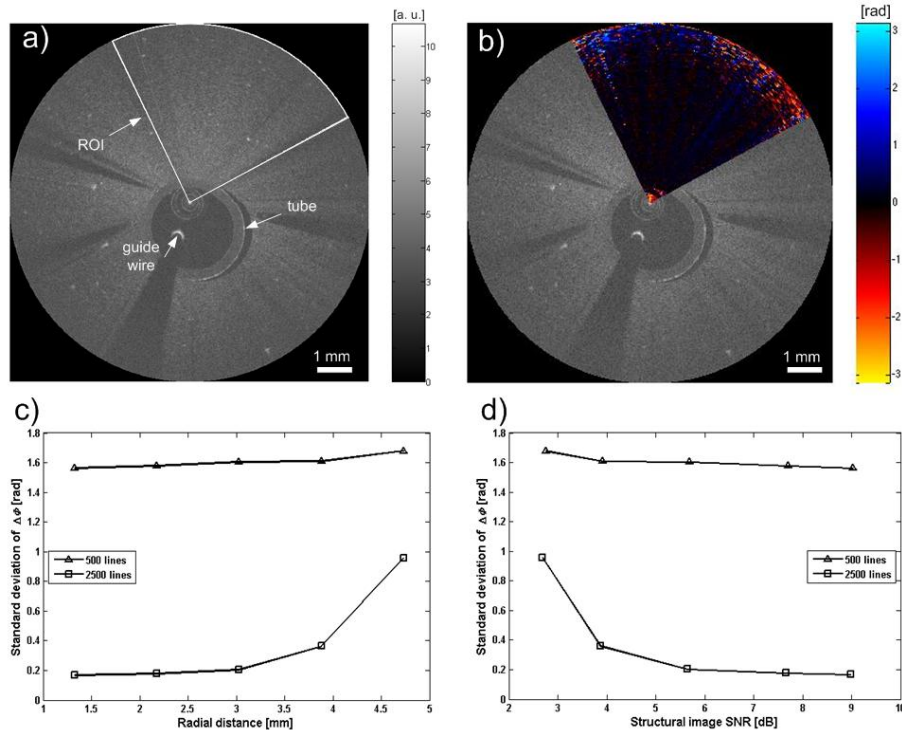

Fig. 4. (a) Structural image of a stationary tissue phantom with TiO_2 particles. White sector represents the ROI. (b) Color Doppler image of the ROI after bulk motion correction. (c) The standard deviation of the Doppler shift changes with radial distance and (d) signal to noise ratio (SNR). The data points in (c) and (d) represent five regions at different radial distances, consisting of 39,600 pixels (2500 A-lines per frame) or 7,920 pixels (500 A-lines per frame). The low SNR phantom is constructed to mimic low SNR of intraluminal blood typically encountered during *in vivo* experiments. The Doppler noise floor increases at the edge of the image with larger radial distance (less voxel overlap between A-lines) and lower SNR.

3. *In vivo* porcine carotid artery imaging

Intravascular flow velocity profiles in porcine carotid arteries were imaged *in vivo* using the above system setup. The *in vivo* porcine carotid imaging procedure presented in this paper has been previously described by our group [20] after adaptation of using 1.5% by volume blood in saline mixture instead of pure saline as the clearing agent injected by an automated pump during Doppler OCT imaging. Briefly a femoral incision was made at the groin of the pig, which was continuously anaesthetized. An 8-French catheter was inserted into the incision as the entry point of the catheter system. Various catheters were used to aid the final insertion of the guide wire and OCT imaging catheter to the carotid artery. Doppler OCT images consisting of 2500 A-lines/frame were taken at a frame rate of 20 frames/s without pullback.

A 3-dimensional reconstruction from pull-back OCT imaging may help to deduce the angle between the catheter axis and the vessel center-line, which may help with better

estimation of the beam to flow angle. Structural images of the vessel wall were first obtained by flushing the blood with pure saline. A 3D structural image of the vessel with catheter and guide wire inside are shown in Fig. 5(a), which shows the catheter is at approximately 10° angle with the vessel wall. The insertion of a catheter into an artery leads to the formation of an annular region between the catheter wall and the arterial wall. A comparison is made with finite element simulation of eccentric annular flow. The simulation is carried out with incompressible and Newtonian fluid with density of 1060 kg/m^3 and viscosity of 0.003 Pa·s. Simulation geometry is set with vessel diameter of 2.5 mm, catheter diameter 0.9 mm, and established laminar flow pattern. The catheter is positioned eccentrically with a gap of 0.2 mm from the vessel wall. The volumetric flow rate applied at the inlet was 5 ml/s, similar to typical saline flush injection rate used for the porcine experiments. The flow profile obtained from the simulation is shown in Fig. 5(b), where the maximum flow is ~57 cm/s.

At the end of flushing when the blood flow mixed with saline images of 500 A-lines/frame and 2500 A-lines/frame were both recorded for Doppler flow measurement. One frame of the structural OCT image of porcine carotid artery consisting of 2500 A-lines is shown in Fig. 5 (c). A seam line appear at the location of the transition between the first and the last A-line due to changes in vessel dimension and relative catheter motion during a cardiac cycle [20]. The longer arrow denotes the guide wire and its artifact. The same cross section imaged by 500 A-lines/frame overlaid with the Doppler signal is shown in Fig. 5(d), where the Doppler shift image shows mainly noise, as expected. In comparison, Figs. 5(e), 5(f) and 5(g) show the 2500 A-lines images, without Doppler artifact removal, with removal, and after applying structural mask to show only the intravascular flow Doppler shift. Due to the high flow velocity in the carotid vessel, the Doppler shift is aliased between [-π, π]. The aliasing pattern within the vessel lumen is distorted by the NURD induced phase artifacts, introducing significant asymmetry in the phase image, as shown in Fig. 5(e). Correction of the phase artifacts, by tracking the phase shift observed on the catheter sheath, significantly reduces the distortion and returns the aliasing contour lines towards the expected pattern. The NURD induced phase artifacts are time variant as shown by video (Media 1) and therefore, frame to frame subtraction will not be sufficient. There are residual phase artifacts which may be greater than those induced by vessel wall motion secondary to arterial pulsation.

A quality-guided phase unwrapping algorithm [21] was used to unwrap the phase map and the corresponding unwrapped phase map is shown in Fig. 5(h). The maximum Doppler shift indicated by '*' is ~24 rad, representing highest blood flow velocity of ~51 cm/s calculated with an estimated Doppler angle of 80°. The arrow indicated area was not unwrapped correctly due to the high shear rate near the wall and Doppler shift noise, which can be observed in (g). The area between the guide wire and the seam line could not be unwrapped properly due to the discontinuity induced by the motion of the catheter and the guide wire. Therefore, this region was not displayed in Fig. 5(h).

In certain clinical settings, it may not be required to phase unwrap the Doppler image, as the aliasing provides natural contour plot of the flow profile. Figure 6 demonstrates a video of simultaneous structural and Doppler OCT imaging of a porcine carotid artery, where dilute (1.5%) blood in saline flush is injected with a contrast injector pump at 5 ml/s (note: typical human carotid angiography uses 4 to 6 ml/s injection rate of contrast). Structural OCT NURD effects can be seen at the 6 to 7 o'clock sector. Seam lines can be seen at 11 to 2 o'clock sector in the Doppler flow images. At the beginning of the video sequence, there is homogenous filling of the vessel lumen by the blood in saline flush, while the vessel wall is still visible. Despite the dilute nature of the flush (1.5% blood by volume), Doppler shift induced by the intravascular flow is clearly visible with associated aliasing rings, which shows the changes of flow waves with time due to changes of flow rate (velocity) [22]. Visibility of the carotid artery wall is affected towards the end of the video sequence, when the injection comes to an end and increased amount of blood starts to fill in the lumen.
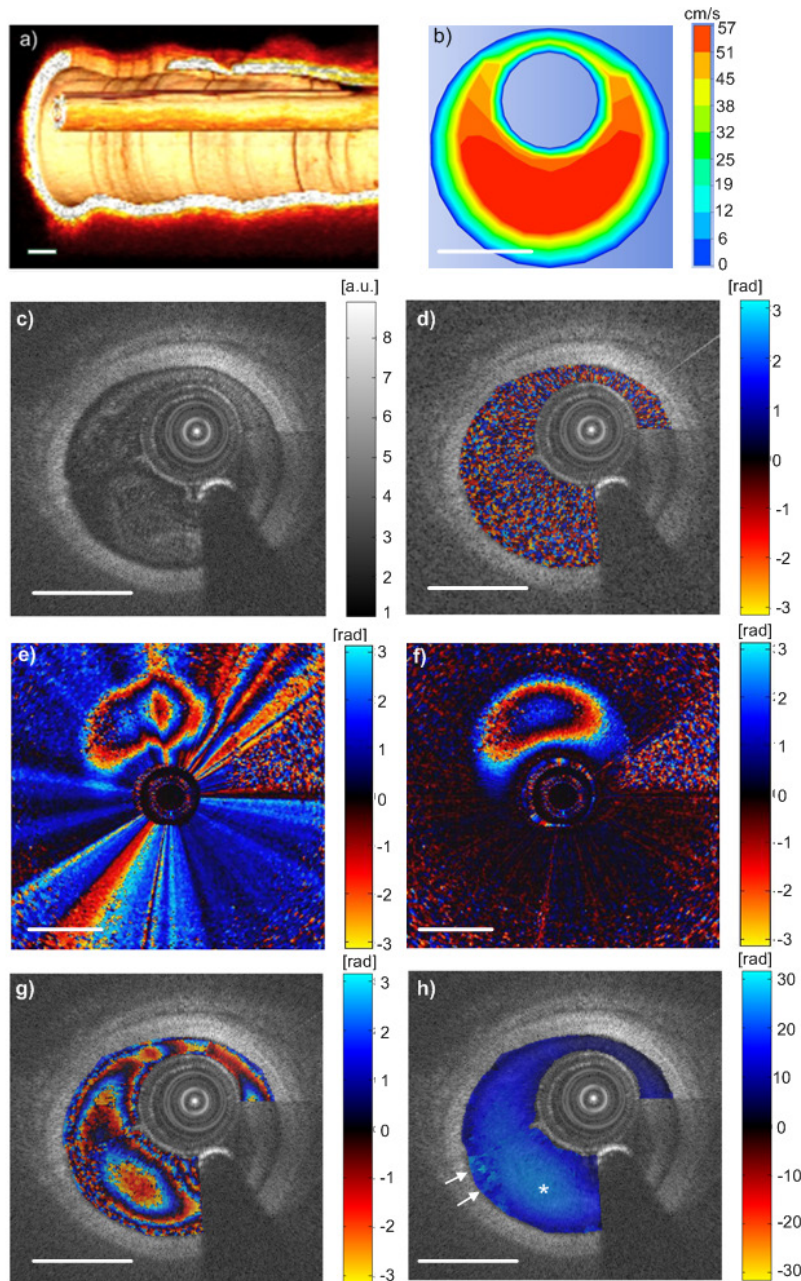
Fig. 5. *In vivo* endovascular flow measurement. (a) 3D OCT image of the catheter and the vessel wall, which shows the angle between the catheter and the wall is ~10°. (b) Simulation results of blood flow. (c) Cross-sectional OCT image of a porcine carotid artery with shadow casted by guide wire. (d) The same cross-section as (c) imaged by 500 A-lines/frame with Doppler shift overlaid, showing mainly noise. (e) and (f) (Media 1). (e) Phase shift image, 2500 A-lines/frame, without NURD induced phase artifact removal. It shows distorted phase contour lines. (f) Phase shift image after NURD induced phase artifact removal by tracking the phase shift in the catheter sheath. The corrected phase contour lines are as expected. The NURD induced artifact is time variant, as shown by Media 1. (g) A typical cross-sectional frame, 2500 A-lines/frame with Doppler shift overlaid, showing aliased phase changes. (h) The unwrapped phase map of (g), where * indicates the highest velocity region. The arrows indicate incorrect phase unwrapping due to noise and high shear rate near the vessel wall. Scale bars = 1 mm.
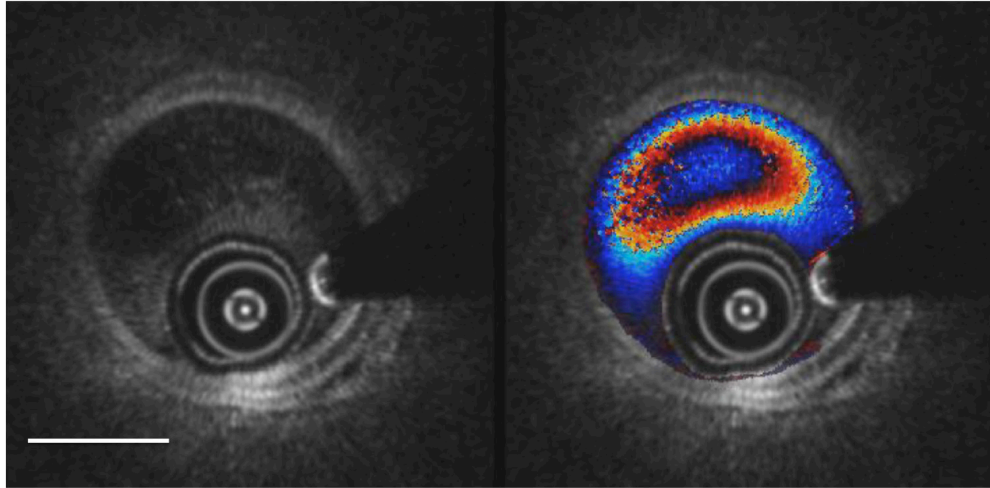
Fig. 6. (Media 2) Simultaneous structural (left) and Doppler overlay (right) OCT video images (Media 2) over 2 seconds during the late phase of pump injection. Note the arterial pulsations in the structural images and the aliasing rings of the flow profile in the Doppler image. A seam line is moving through between the 11 o'clock and 2 o'clock positions, more apparent in the Doppler image than the structural. Scale bar = 1 mm.

4. Discussion and conclusion

While multiple different scanning protocols for phase resolved Doppler OCT flow imaging in the Cartesian coordinate have been introduced in the recent years [23,24], especially with the advance of increased A-scan rates available via high speed swept wavelength lasers or line-scan cameras and galvoscanners, rotational catheter based phase resolved Doppler OCT for intravascular flow is less developed. Frame to frame phase shift calculation is not reliable with fiber rotational speed of 100 rps during *in vivo* imaging. Therefore, line-to-line phase calculation needs to be employed, yet 50 to 100 kHz A-scan rate limits the frame rate since sufficient A-scan density is required for Doppler imaging. In this work, the imaging was conducted at a frame rate of 20 frames/s with 2500 A-lines/frame, which is the optimized condition for this particular endovascular OCT system. Theoretically the denser the A lines the better Doppler signal can be detected. As the rotating speed of the catheter is 20 rounds/s, the maximum A lines per frame is 2500 for the 50 KHz endovascular OCT system. Thus the animal trials were conducted with 2500 A-lines/frame imaging. The laser, rotary mechanism of the catheter, and the physiological characteristics being imaged, need to be considered simultaneously to determine an optimized condition for a particular application.

Currently the minimum detectable flow velocity determined by the noise floor of the Doppler shift shown in Fig. 3(a) is ~2 mm/s, assuming a Doppler angle of 70°. The maximum detectable velocity, when multiple aliasing rings are visible, is affected by a combination of factors including SNR, spatial resolution, and the performance of the phase unwrapping techniques. In principle, phase unwrapping technique breaks down when the velocity gradient equivalent to 2π occurs over a spatial dimension comparable to the resolution of the OCT system [25]. In practice, reduced SNR due to the low scattering flush fluid (1.5% blood in saline) will further decrease the maximal detectable velocity. The finite element simulation provided similar results with real-time intravascular imaging as shown in Fig. 5, demonstrating measurement of absolute flow velocity at 51 cm/s.

We note the simulation contains assumptions including non-deformable straight tube with homogenous material properties, fluid density and viscosity of blood. These depart from biological tissue with visco-elastic properties and responds to pressure wave propagation from the arterial pulse. Many other factors, such as scatterer concentration and tissue scattering

parameters [26] affect the OCT signal and Doppler flow profile measurement. The main source of error, however, arises from inability to precisely define the Doppler angle in this work. Under *in vivo* conditions with catheter bending within pulsating vessel, 10° angular error will not be an over estimation as observed from real-time angiography. Therefore, future Doppler measurement accuracy improvement can be obtained by conical rotational scanning.

In comparison to IVUS based Doppler methods for intravascular flow imaging, Doppler OCT provides better spatial and velocity resolution as both technique are subjected to the same Doppler angle error, but optical wavelength is much shorter than IVUS even when the latter operates at 100 MHz. OCT suffers from the need to optically clear the blood while imaging, hence the pump injector may distort the intravascular flow profile from physiological states. We note, however, during most catheter based interventional procedures, the multiple devices inside the vessel (e.g., guide catheter, imaging catheter, guide wires, etc.) would have already significantly altered the flow profile. Directly imaging changes during different stages of interventional treatment, such as those before and after angioplasty or stenting, will provide insights to clinical applications, especially considering subtle changes of the vessel in geometry can affect the flow field significantly [27].

In conclusion, simultaneous structure OCT imaging and Doppler flow measurement in porcine carotid artery was demonstrated, after investigating the required A-scan density and NURD induced phase shift artifact. Using an endovascular OCT system with custom-built data acquisition system and phase shift artifact removal algorithm, minimal detectable velocity was characterized in a slow flow phantom. To our knowledge, this is the first *in vivo* demonstration of Doppler imaging and absolute measurement of intravascular flow using a rotating fiber catheter in carotid artery.

Acknowledgments